Available online at www.sciencedirect.com
ScienceDirect
Progress in Particle and Nuclear Physics 59 (2007) 74–93
Progress in Particle and Nuclear Physics
www.elsevier.com/locate/ppnp

Review

Production of intermediate-mass and heavy nuclei

F.-K. Thielemann[a,*], C. Fröhlich[a], R. Hirschi[a], M. Liebendörfer[a], I. Dillmann[a], D. Mocelj[a], T. Rauscher[a], G. Martinez-Pinedo[b], K. Langanke[b], K. Farouqi[c], K.-L. Kratz[c], B. Pfeiffer[c], I. Panov[d], D.K. Nadyozhin[d], S. Blinnikov[d], E. Bravo[e], W.R. Hix[f], P. Höflich[g], N.T. Zinner[h]

[a] *Department of Physics and Astronomy, University of Basel, Switzerland*
[b] *Gesellschaft für Schwerionenforschung (GSI), Darmstadt, Germany*
[c] *Institute for Nuclear Chemistry, University of Mainz and Max Planck Institute for Chemistry, Mainz, Germany*
[d] *Institute for Theoretical and Experimental Physics, Moscow, Russia*
[e] *Departament de Física, Universitat Politècnica de Catalunya, Barcelona, Spain*
[f] *Physics Division, Oak Ridge National Laboratory, Oak Ridge, TN 37831, USA*
[g] *Department of Physics, Florida State University, Tallahassee, FL 32306, USA*
[h] *Institute for Physics and Astronomy, University of Arhus, Denmark*

Abstract

Nucleosynthesis is the science related to all astrophysical processes which are responsible for the abundances of the elements and their isotopes in the universe. The astrophysical sites are the big bang and stellar objects. The working of nucleosynthesis processes is presented in a survey of events which act as abundance sources. For intermediate-mass and heavy elements, these are stellar evolution, type Ia and core collapse supernovae as well as hypernovae. We discuss successes and failures of existing processes and possible solutions via new (hitherto unknown) processes. Finally an analysis of their role is given in the puzzle to explain the evolution of the elemental and isotopic compositions found in galaxies, and especially the mixture found in the solar system. Different timescales due to the progenitor mass dependence of the endpoints of stellar evolution (type II supernova explosions — SNe II vs. planetary nebulae) or single vs. binary stellar systems (the latter being responsible for novae, type Ia supernovae — SNe Ia, or X-ray bursts) are the keys to understand galactic evolution. At very early times, the role of explosion energies of events, polluting pristine matter with a composition originating only from the big bang, might also play a

* Corresponding author.
E-mail address: F-K.Thielemann@unibas.ch (F.-K. Thielemann).

0146-6410/$ - see front matter
doi:10.1016/j.ppnp.2006.12.019

role. We also speculate on the role of very massive stars not undergoing SN II explosions but rather causing "hypernovae" after the formation of a central black hole via core collapse.

Keywords: Nuclear reactions; Neutrino–nucleus interactions; Nuclear structure; Fission; Stellar evolution; Nucleosynthesis; Type Ia supernovae; Core collapse supernovae; Si-burning; r-process; *νp*-process; p-process; Chemical evolution of galaxies; Low metallicity stars

1. Introduction

The sites of stellar nucleosynthesis span stable (hydrostatic) stellar evolution and wind ejection [30,62] as well as explosions like novae and both types of supernovae [107,89,54,11, 12,90,96,39] hypernovae/gamma-ray bursts [104,72,70,7] or possibly other events, where binary stellar systems are involved. The understanding of each of these environments requires in general hydro (fluid/gas) dynamics, thermodynamics, energy transport [55,12] and last but not least, the knowledge of nuclear physics comprising nuclear reactions, nuclear structure and decay properties [45,51] as well as the nuclear equation of state [52]. Thermonuclear burning, nuclear energy generation and resulting nuclear abundances are determined by thermonuclear and weak interaction rates. Before reviewing hydrostatic burning phases in stellar evolution, the specific burning features of explosive stellar events, astrophysical sites and their contribution to galactic evolution, we want to outline briefly the essential features of thermonuclear reaction rates and the basic equations governing composition change in nuclear reaction networks, and the required nuclear physics input.

In general, when targets j and projectiles k follow specific thermal momentum distributions $\mathrm{d}n_j$ and $\mathrm{d}n_k$ in an astrophysical plasma, leading to relative velocities $\vec{v}_j - \vec{v}_k$, r, the number of reactions per cm^3 and sec, is given by

$$r_{j,k} = \int \sigma(|\vec{v}_j - \vec{v}_k|)|\vec{v}_j - \vec{v}_k|\,\mathrm{d}n_j\,\mathrm{d}n_k.$$

The evaluation of this integral depends on the type of particles (fermions, bosons) and distributions which are involved. For nuclei j and k in an astrophysical plasma obeying a Maxwell–Boltzmann distribution, this simplifies to $r_{j,k} = \langle\sigma v\rangle n_j n_k$. The thermonuclear reaction rates have the form

$$\langle\sigma v\rangle_{j,k} = \left(\frac{8}{\mu\pi}\right)^{\frac{1}{2}} (kT)^{-\frac{3}{2}} \int_0^\infty E\sigma(E)\mathrm{e}^{-E/kT}\mathrm{d}E.$$

Here μ and E denote the reduced mass and center of mass energy of the target-projectile system. When particle k is a photon, the relative velocity is always c and the quantities in the integral are not dependent on $\mathrm{d}n_j$. This simplifies to $r_j = \lambda_{j,\gamma} n_j$. $\lambda_{j,\gamma}(T)$ results from an integration over a Planck distribution for photons of temperature T.

A similar procedure is used for electron captures by nuclei. Because the electron is about 2000 times less massive than a nucleon, the velocity of the nucleus j is negligible in the center of mass system in comparison to the electron velocity ($|\vec{v}_j - \vec{v}_e| \approx |\vec{v}_e|$). The electron capture cross section has to be integrated over a or Fermi distribution of electrons. The electron capture rates are a function of T and $n_e = Y_e \rho N_\mathrm{A}$, the electron number density, where ρ denotes the matter density and N_A Avogadro's number. In a neutral, completely ionized plasma, the electron

abundance is equal to the total proton abundance $Y_e = \sum_i Z_i Y_i$ and $r_j = \lambda_{j,e}(T, \rho Y_e) n_j$. The abundances Y_i are defined below.

This treatment can be generalized for the capture of positrons, which are in a thermal equilibrium with photons, electrons, and nuclei. At high densities ($\rho > 10^{12}$ g cm^{-3}), the size of the neutrino scattering cross section on nuclei and electrons ensures that enough scattering events occur to thermalize a neutrino distribution. Then the inverse process to electron capture (neutrino capture) can also occur and be expressed similarly to photon and electron captures, integrating now over the neutrino distribution. Finally, for normal decays with half-life $\tau_{1/2}$, we obtain an expression with the decay rate $\lambda_j = \ln 2/\tau_{1/2}$ independent of temperature or density.

The time derivative of the number densities of each of the species in an astrophysical plasma is governed by the different expressions for r, as discussed above for the different reaction mechanisms belonging to the three categories of reactions: (1) decays, photodisintegrations, electron and positron captures and neutrino induced reactions ($r_j = \lambda_j n_j$), (2) two-particle reactions ($r_{j,k} = \langle j,k\rangle n_j n_k$), and (3) three-particle reactions ($r_{j,k,l} = \langle j,k,l\rangle n_j n_k n_l$) like the triple-alpha process, which can be interpreted as successive captures with an intermediate unstable target. In order to exclude changes in the number densities $\dot{n}_i$, which are only due to expansion or contraction of the gas, the nuclear abundances $Y_i = n_i/(\rho N_\mathrm{A})$ were introduced, where A_i, $A_i Y_i$ represent the atomic weight and the mass fraction of this nucleus. In terms of abundances Y_i, we obtain a set of differential equations

$$\dot{Y}_i = \sum_j N^i_j \lambda_j Y_j + \sum_{j,k} N^i_{j,k} \rho N_\mathrm{A} \langle j,k\rangle Y_j Y_k + \sum_{j,k,l} N^i_{j,k,l} \rho^2 N_\mathrm{A}^2 \langle j,k,l\rangle Y_j Y_k Y_l.$$

The captital N's indicate how many nuclei of type i are destroyed ($-$) or produced ($+$) in the corresponding reaction. This reaction network has, in general, to be solved numerically. A simplified situation is given in case of a nuclear statistical equilibrium (NSE) at high temperatures. Instead of solving reaction networks, which would result in the same, but much more time consuming, solution, the abundances can be expressed by a chemical equilibrium for the build-up of all nuclei from neutrons and protons via the chemical potentials $\mu(Z,A) = Z\mu_p + (A-Z)\mu_n$. With typical Boltzmann distributions this leads to

$$Y_i = (\rho N_\mathrm{A})^{A_i - 1} \frac{G_i}{2^{A_i}} A_i^{\frac{3}{2}} \left(\frac{2\pi\hbar^2}{m_u kT}\right)^{\frac{3}{2}(A_i-1)} \mathrm{e}^{B_i/kT} Y_p^{Z_i} Y_n^{N_i},$$

for the abundance of nucleus Y_i, with nuclear binding energy B_i and partition function $G_i(T)$. The required solution for neutron and proton abundances Y_n and Y_p is found from mass conservation $\sum_i A_i Y_i = 1$ and charge conservation $\sum_i Z_i Y_i = Y_e$. In that case, only the slow weak interaction processes, which change Y_e as a function of time, have to be followed explicitly.

The total energy generation rate per gram, due to nuclear reactions with abundance changes $\dot{Y}_i$, is expressed in terms of the rest mass $M_i c^2$ of the participating nuclei

$$\dot{\epsilon} = -\sum_i \dot{Y}_i N_\mathrm{A} M_i c^2.$$

As noted above, the important ingredients for nucleosynthesis calculations are decay half-lives, electron and positron capture rates, photodisintegrations, neutrino induced reaction rates, and strong interaction cross sections. Photodisintegration rates can be calculated via detailed balance from the reverse capture rates. For recent surveys related to experiments or light nuclei see [45,1,6,43,51,58,29,10]. Theoretical investigations are presented in [79–81,16,2]. The latest

status of weak interaction rates (including electron and neutrino reactions) is given in [50,48,26]. Beta half-life predictions for heavy nuclei are discussed in [63,8]. A survey of computational methods to solve nuclear networks is given in [33].

2. Hydrostatic and explosive burning

Nuclear burning can, in general, be classified into two categories: (1) hydrostatic burning stages on timescales dictated by stellar energy loss, and (2) explosive burning due to the hydrodynamics of the specific event. Hydrostatic burning stages are characterized by temperature thresholds, permitting thermal Maxwell–Boltzmann distributions of (charged) particles (nuclei) to penetrate increasingly larger Coulomb barriers of electrostatic repulsion. H-burning converts of ^{1}H into ^{4}He via pp-chains or the CNO-cycles. The simplest pp-chain is initiated by $^{1}\mathrm{H(p,e^{+}\nu)}\,^{2}\mathrm{H(p,\gamma)}\,^{3}\mathrm{He}$ and completed by $^{3}\mathrm{He}(^{3}\mathrm{He},2\mathrm{p})^{4}\mathrm{He}$. The dominant CNO-cycle chain $^{12}\mathrm{C(p,\gamma)}\,^{13}\mathrm{N(e^{+}\nu)}\,^{13}\mathrm{C(p,\gamma)}\,^{14}\mathrm{N(p,\gamma)}\,^{15}\mathrm{O(e^{+}\nu)}\,^{15}\mathrm{N(p,\alpha)}\,^{12}\mathrm{C}$ is controlled by the slowest reaction $^{14}\mathrm{N(p,\gamma)}\,^{15}\mathrm{O}$. Further burning stages are characterized by the major reactions, which are in He-burning [$^{4}\mathrm{He}(2\alpha,\gamma)\,^{12}\mathrm{C}$ (triple-alpha) and $^{12}\mathrm{C}(\alpha,\gamma)\,^{16}\mathrm{O}$], in C-burning [$^{12}\mathrm{C}(^{12}\mathrm{C},\alpha)\,^{20}\mathrm{Ne}$], and in O-burning [$^{16}\mathrm{O}(^{16}\mathrm{O},\alpha)\,^{28}\mathrm{Si}$]. These features, key reactions and the status of nuclear cross sections are discussed in recent reviews on hydrostatic burning stages [29, 10]. The alternative to fusion reactions are photodisintegrations which start to play a role at sufficiently high temperatures T when $30kT \approx Q$ (the Q-value or energy release of the inverse capture reaction). This ensures the existence of photons with energies $> Q$ in the Planck distribution and leads to Ne-Burning [$^{20}\mathrm{Ne}(\gamma,\alpha)\,^{16}\mathrm{O}$, $^{20}\mathrm{Ne}(\alpha,\gamma)\,^{24}\mathrm{Mg}$] at $T > 1.5 \times 10^{9}$ K (preceding O-burning) due to a small Q-value of ≈4 MeV and Si-burning at temperatures in excess of 3×10^{9} K [initiated like Ne-burning by photodisintegrations]. The latter ends with nuclear reactions in a complete chemical equilibrium (nuclear statistical equilibrium, NSE) and an abundant distribution around Fe. These temperatures permit photodisintegrations with typical Q-values of 8–10 MeV as well as the penetration of Coulomb barriers in capture reaction. In such an NSE, the abundance of each nucleus Y_i is only dependent on temperature T, density ρ, its nuclear binding energy B_i, and via charge conservation on $\sum_i Z_i Y_i = Y_e$ as discussed in the preceding section. Y_e is changed by weak interactions on longer timescales. Quasi-equilibrium can occur when different nuclear mass regions, usually separated by small Q-values, are in equlibrium with the background of free neutrons, protons and alphas, but offset from their NSE values [34,33].

During core and shell He-burning, specific α-induced reactions can liberate neutrons which are responsible for the slow neutron capture process (s-process). It leads to the build-up of elements up to Pb and Bi through a series of neutron captures and β^{-}-decays, starting on existing heavy nuclei around Fe [46]. Many of the hydrostatic burning processes occur also under explosive conditions at higher temperatures and on shorter timescales (see Fig. 1), when often the β-decay half-lives are longer than the explosive timescales. This requires, in general, additional knowledge of nuclear reactions for unstable nuclei. The fuels for explosive nucleosynthesis consist mainly of $N = Z$ nuclei like ^{12}C, ^{16}O, ^{20}Ne, ^{24}Mg, or ^{28}Si (the ashes of prior hydrostatic burning), resulting in heavier nuclei, again with $N \approx Z$. At high densities substantial electron captures on nuclei $\mathrm{e}^{-} + {}^{A}Z \rightarrow {}^{A}Z - 1 + \nu$ can also occur due to energetic, degenerate electrons with high Fermi energies (equivalent to a β^{+}-decay which converts a proton into a neutron inside a nucleus).

Explosive Si-burning differs strongly from its hydrostatic Counterpart, and can be divided into three different regimes: (i) incomplete Si-burning and complete Si-burning, with either (ii)

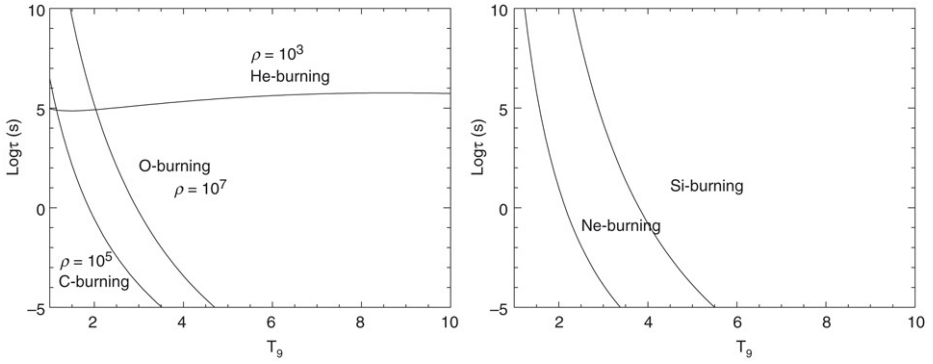

Fig. 1. Burning timescales in seconds for fuel destruction of He-, C-, and O-burning (left) and Ne- and Si-burning (right) as a function of temperature. Density-dependent timescales are labeled with a chosen typical density (in g cm^{-3}). They scale with $1/\rho$ for C- and O-burning and $1/\rho^2$ for He-burning. Ne- and Si-burning, initiated by photodisintegrations, are not density-dependent. The almost constant He-burning timescale beyond $T_9 = T/10^9$ K = 1 permits efficient destruction on explosive timescales only for high densities.

a normal (high density, low entropy,) or (iii) an alpha-rich (low density, high entropy) freeze-out of charged-particle reactions during cooling from NSE. At high temperatures or during a "normal" freeze-out, the abundances remain in a full NSE. The full NSE can break up in smaller equilibrium clusters (quasi-equilibrium, QSE), for a detailed discussion see [34,33]. An example for such QSE-bevavior is an alpha-rich freeze-out, caused by the inability of the triple-alpha reaction ^{4}He$(2\alpha,\gamma)\,^{12}$C, and the ^{4}He$(\alpha n,\gamma)\,^9$Be to keep light nuclei like n, p, and ^{4}He, and nuclei beyond $A = 12$ in an NSE during declining temperatures, when the densities are small. This causes a large alpha abundance after freeze-out. This effect, most pronounced for SNe II, is a function of entropy being proportional to T^3/ρ in a radiation dominated plasma (see Fig. 2).

r-process nucleosynthesis (rapid neutron capture) relates to subsets of explosive Si-burning, either with low or high entropies, experiencing a normal or alpha-rich freeze-out. The requirement of a neutron/seed ratio of 10–150 after charged particle freeze-out translates for a normal freeze-out into $Y_e = 0.12$–0.3. For a moderate $Y_e > 0.40$, an extremely alpha-rich freeze-out is needed (see the disussion in Section 5).

3. The evolution of stars

3.1. Massive stars and supernovae

For the evolution of single stars in the Hertzsprung–Russell (HR) diagram, see e.g. [42]. Their fate is mainly determined by their initial mass and composition. This implies, in principle, also the history of mass loss, but in theoretical modeling, the mass loss prescription adds a degree of freedom. Rotation can drastically affect the evolutionary track of a star in the HR diagram due to the modification of its surface composition, induced by rotational diffusion, which directly affects the mass loss by stellar winds. The mass loss rates depend on metallicity via the interaction of radiation transport with the surface composition. The present theoretical and observational knowledge is summarized in [62]. In general, this leads to low metallicity stars experiencing less mass loss than high metallicity stars, and therefore possessing larger He cores and H envelopes at the end of their lives. The same applies to the C–O-core size after He-burning, which determines the final fate of the star, due to the much shorter burning timescales of the later burning stages (see Fig. 3(a)).

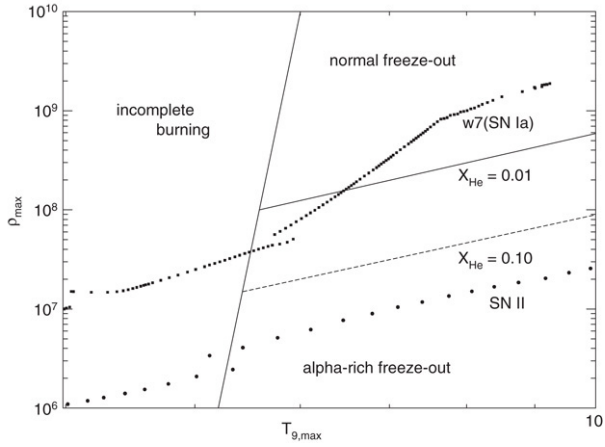

Fig. 2. Final results of explosive Si-burning as a function of maximum temperatures and densities attained in explosions before adiabatic expansion. For temperatures in excess of 5×10^9 K, any fuel previously existing is photodisintegrated into nucleons and alpha particles before re-assembling in the expansion. For high densities, this is described by a full NSE prevailing until freeze-out at about $2–3 \times 10^9$ K, which results in an Fe-group composition according to maximum binding energies for nuclei with the global neutron/proton ratio of the plasma (or Y_e, the total proton to nucleon ratio). For lower densities, the NSE breaks into local equilibrium groups (quasi-equilibrium, QSE), with group boundaries determined by reactions with an insufficiently fast reaction stream required for an NSE. Alpha-rich freeze-out (insufficient conversion of alpha-particles into nuclei beyond carbon) is such a QSE-behavior. Lines with 1% and 10% remaining alpha mass fraction are indicated, as well as typical conditions in type Ia and type II supernova mass zones.

For different initial masses and metalicities, different end stages, like e.g. white dwarfs, supernovae and black holes (hypernovae, gamma-ray bursts) can be expected. The lower boundary for stars to form massive enough cores to undergo core collapse is at $\sim$9 $M_\odot$. For stars above 10 $M_\odot$, core collapse is the only possible fate [30,70]. In between, stars form O–Ne–Mg cores, which can either collapse and form a neutron star or lose their envelope and result in a white dwarf. While the size of the C–O-core determines the final stellar fate, its relation to the progenitor mass depends on its metallicity. At low metalicities, massive stars end their lives either as neutron stars (for initial mass of $\sim$10 $M_\odot$–40 $M_\odot$, as black holes through fallback onto the neutron star (initial mass between $\sim$25 $M_\odot$ and $\sim$40 $M_\odot$), or directly as black holes (initial mass above $\sim$40 $M_\odot$) [32,70,104,72,7]. At higher metalicities, mass loss becomes more important, producing smaller He and C/O-cores for a given initial mass. For very massive stars the metallicity dependence can be so strong that with increasing metalicity the mass loss during stellar evolution is large enough to exclude black hole formation, permitting neutron stars as the only possible type of remnant.

Core collapse with neutron star formation leads to supernovae (dependent on observations of H- and/or He-lines divided into subclasses of type II and type Ib or Ic). For a recent summary see [30]. Fig. 3(b) shows the resulting explosion energy for solar metallicities from the calculations discussed in Section 5 [54]. For the general working of the SN II mechanism see also [11,59,12].

Type Ia supernovae show, in addition to the absence of hydrogen in their optical spectra, a specific Si-line. They are the only type of supernovae observed in elliptical galaxies, and therefore have to originate from an older (revived) stellar population. Their origin is explained via exploding carbon–oxygen white dwarfs in binary stellar systems after accreting sufficient matter from the companion star to undergo a thermonuclear runaway (see Section 4).

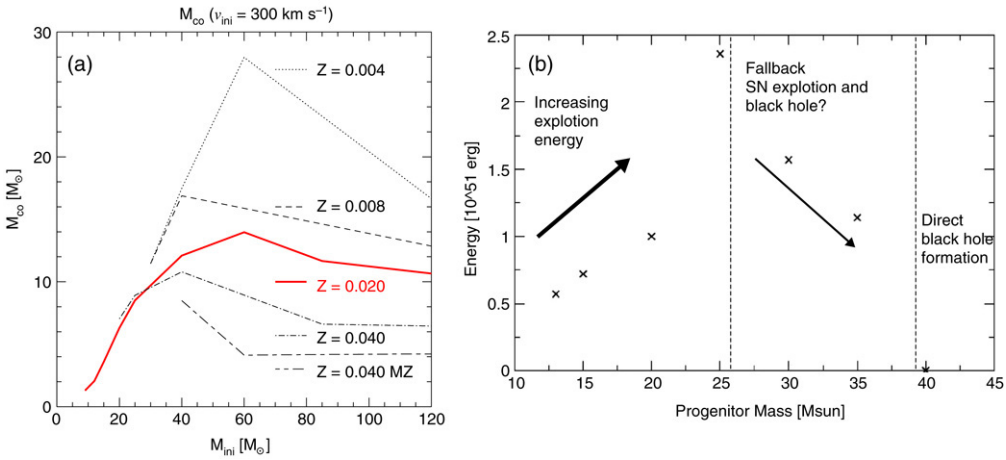

Fig. 3. *Left panel:* CO core masses from stellar evolution calculations for different metalicities (mass fraction of elements including and beyond C) as function of the initial stellar mass [32]. *Right panel:* Explosion energy as function of progenitor mass for core collapse supernovae (of solar metallicity) due to neutrino absorption. The explosion energy shows a peak around ∼25 $M_\odot$, increasing with increasing progenitor mass at lower masses and decreasing fast for higher masses. Above ∼40 $M_\odot$ no explosions are observed [54].

3.2. Low mass stars, the s-process, and the s-, r-, p- decomposition of heavy elements

Low and intermediate mass stars, which enrich the interstellar medium via stellar winds and/or planetary nebula ejection before forming central C+O white dwarfs, contribute important amounts of He and C as well as other H- and He-burning products. Among the He-burning products, one also finds about half of the heavy elements and isotopes beyond Fe and up to Pb and Bi, resulting from s-process nucleosynthesis, which is due to neutron capture an pre-existing intermediate and heavy nuclei. In core and shell He-burning neutrons are provided by a side branch of He-burning reactions acting on ^{14}N, the dominant CNO nucleus after H-burning: $^{14}\mathrm{N}(\alpha,\gamma)\,^{18}\mathrm{F}(\mathrm{e}^{+}\nu)\,^{18}\mathrm{O}(\alpha,\gamma)\,^{22}\mathrm{Ne}(\alpha,\mathrm{n})\,^{25}\mathrm{Mg}$. An alternative stronger neutron source during the period of He-shell flashes in low and intermediate mass stars is the reaction $^{13}\mathrm{C}(\alpha,\mathrm{n})\,^{16}\mathrm{O}$, which requires admixture of hydrogen and the production of ^{13}C via $^{12}\mathrm{C}(\mathrm{p},\gamma)\,^{13}\mathrm{N}(\mathrm{e}^{+}\nu)\,^{13}\mathrm{C}$. The s-process is characterized by neutron captures, which are slow in comparison to beta-decays [46,86].

Fig. 4 shows a section of the chart of nuclei and the s-process path indicated by horizontal arrows for neutron captures with reaction rates $\langle\sigma v\rangle_{n,\gamma}(A) \equiv \langle\sigma v\rangle_{\mathrm{A}}$, connected by β^--decays whenever an unstable nucleus is encountered. The path can be simplified by abundances related only to mass numbers A, and the abundances approach a steady flow equilibrium $\dot{Y}_{\mathrm{A}} = 0$ of creation and distruction. For a large fraction of nuclei, the neutron cross sections scale with $E^{-1/2}$ ($l = 0$ s-wave capture), which causes a temperature independent $\langle\sigma v\rangle$. Then the resulting abundance pattern is only dependent on the neutron exposure $\tau = \int n_n \,\mathrm{d}t$. There exist two complications to the simple picture given above: (i) nuclei with very long β-decay half-lives (comparable to the s-process duration time) can cause branchings into two flows, and (ii) cross sections which are not s-wave dominated. These lead to a temperature dependent $\langle\sigma v\rangle$. In that case the results are not just a function of τ, but can depend on $n_n(t)$ and $T(t)$.

The s-process is recognized to occur in at least two different astrophysical sites, the weak component accounting for most of the s-nuclei below the Kr–Rb–Sr abundance peak, and the

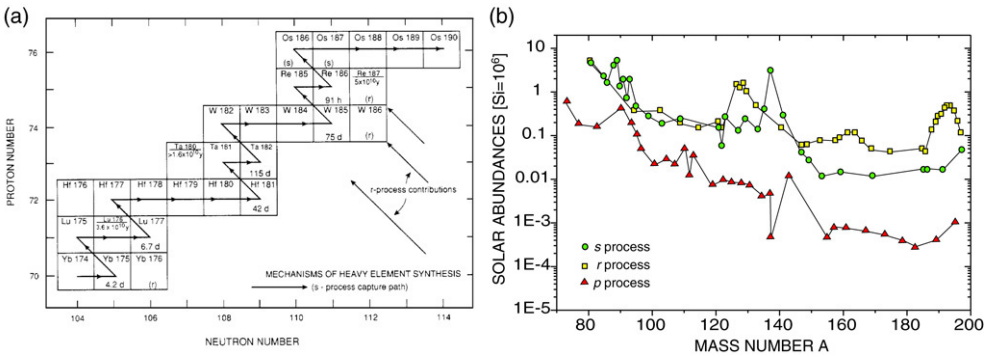

Fig. 4. *Left panel:* A typical portion of the nuclear chart for heavy elements beyond the "Fe-group". The s-process path, which is constrained to the "valley" of stability, is indicated. Neutron-rich r-only isotopes formed by the r-process are identified, as well as the shielded s-only isotopes, which cannot have an r-process contribution. Stable isotopes, more proton-rich than the s-process path, have typically an abundance smaller by two orders of magnitude than s- and r-isotopes. Their origin is due to the p- or γ-process. *Right panel:* Decompositions of solar s-process, r-process and p-process abundances [5,46,99]. Notice the opposite behavior of the s- and r-process with respect to odd–even staggering.

main component accounting for heavier nuclei up to Pb. The main s-process component is due to the thermally-pulsing phase of shell He- and H-burning in low mass stars ($M \leq 3\ M_{\odot}$), and primarily driven by $^{13}C(\alpha, n)\,^{16}O$ rather than $^{22}Ne(\alpha, n)\,^{25}Mg$. Recent research indicates that $^{13}C(\alpha, n)\,^{16}O$ burns in the interpulse phases at low temperatures. Core He-burning with the ^{22}Ne source contributes to the weak s-component, which is a complex combination of core He-, and shell C-, and Ne-burning in massive stars. Further detailed discussions can be found with respect to the nuclear physics input [46], stellar models [86] as well as abundance determinations from isotopic anomalies in meteorites (originating from dust formed in stellar winds) [103].

Understanding the s-process composition can also provide the r-process abundances (see Section 5) by subtracting the s-process component from the total solar abundances for those nuclei which have s- and an r-contributions (see Fig. 4(a), (b)). The s- and r-process contributions have abundance peaks related to closed neutron shells ($N = 50, 82, 126$ for $A = 88, 138,$ and 208), either in the stability valley where small cross sections are encountered or far from stability where long beta half-lives are encountered [46,15,22]. In a similar fashion, the p-process component is obtained for the proton-rich nuclei. The p-process [99] and r-process [87,105,91] are identified with a supernova origin.

4. Type Ia supernovae

There are strong theoretical and observational indications that SNe Ia are thermonuclear explosions of accreting white dwarfs in binary systems [36,71,67,37,90,39]. The basic idea is simple: a white dwarf in a binary system grows towards the Chandrasekhar mass limit through accretion of material from the companion. The contraction and central carbon ignition cause a thermonuclear runaway, since the pressure is dominated by a degenerate electron gas and shows no temperature dependence. This prevents stable and controlled burning, causing a complete explosive disruption of the white dwarf [69,106]. The mass accretion rate determines the central ignition density in spherically symmetric models. However, the initial white dwarf mass, its C/O ratio, and its metallicity might enter as well [40,98,38,17,39]. In addition, rotation and multi-D effects complicate the situatioan, see e.g. [96].

The flame front propagates initially at a subsonic speed as a deflagration wave due to heat transport across the front [31,83,84]. The averaged spherical flame speed depends on the development of instabilities of various scales at the flame front. Multi-dimensional hydro simulations suggest a speed $v_{\rm def}$ as slow as a few percent of the sound speed v_s in the central region of the white dwarf. Electron capture affects the central electron fraction Y_e and depends on (i) the electron capture rates of nuclei [49], (ii) $v_{\rm def}$, influencing the time duration of matter at high temperatures (and with it the availability of free protons for electron captures), and (iii) the central density of the white dwarf $\rho_{\rm ign}$ (increasing the electron chemical potential i.e. the Fermi energy) [44,9]. After an initial deflagration in the central layers, the deflagration might turn into a detonation (supersonic burning front) at larger radii and lower densities [47,66]. This is debated [83,84], but leads to a more consistent picture with observations [39]. The transition from a deflagration to a detonation (delayed detonation model) leads to a change in the ratios of Si-burning sub-categories with varying entropies. This also leaves an imprint on the Fe-group composition.

Explosive nucleosynthesis calculations in spherical symmetry for slow deflagrations, followed by a delayed detonation or a fast deflagration, are used to investigate the constraints on the parameters $\rho_{\rm ign}$, $v_{\rm def}$, and the transition density. Variations in the ignition density $\rho_{\rm ign}$ and the initial deflagration velocity $v_{\rm def}$ affect the Fe-group composition in the central part. The effect of different models on the maximum temperature and density during the Si-burning of the central layers, obtained during the propagation of the burning front, is discussed in [44].

The ignition density $\rho_{\rm ign}$ affects the electron Fermi energy and dominates the amount of electron capture, and thus Y_e in the central layers. The deflagration speed $v_{\rm def}$ determines the resulting Y_e-gradient as a function of the radius. During the burning, the central region undergoes electron captures on free protons and on Fe-peak nuclei. Similar central densities with higher temperatures lead (via the more energetic Fermi distributions of electrons and also the larger NSE-abundances of free protons) to larger amounts of electron capture, and therefore smaller central Y_e values [44,9,90] (see Fig. 5).

Most of the central region experiences conditions for complete Si-burning and subsequent normal (or alpha-rich) freeze-out. The main nucleosynthesis products are Fe-group nuclei. The outer part of the central region undergoes incomplete Si burning (due to lower peak temperatures), and therefore has Ca and other alpha elements as main products. The total nucleosynthesis yields in slow deflagration models show that the production of Fe-group nuclei in comparison to their solar values is a factor of 2–3 larger than the production of intermediate nuclei from Si to Ca [44,9,90].

There are some Fe-group contributions from alpha-rich freeze-out and incomplete Si-burning layers that depend on the deflagration–detonation–transition. The mass region experiencing incomplete Si-burning (dominated by ^{54}Fe) decreases with decreasing transition density. The region experiencing alpha-rich freeze-out (dominated by ^{58}Ni) increases with decreasing transition density. ^{52}Fe (decaying to the dominant Cr isotope ^{52}Cr) and ^{55}Co (decaying to the only stable Mn isotope ^{55}Mn) are typical features of incomplete Si burning. ^{59}Cu (decaying to the only stable Co isotope ^{59}Co) is a typical feature of an alpha-rich freeze-out.

Generally speaking, to the first order we do not expect these main features to change with galactic evolution or metallicity. The main Fe-group composition is determined by the Y_e resulting from electron captures in the explosion. The Y_e of the outer layers are affected by electron captures, depending mildly on the initical CNO (i.e. metallicity). However, secondary effects like (a) the main sequence mass distribution of the progenitors (determining the C–O-core from core He-burning and the C–O-layers from burning during the accretion phase), (b)

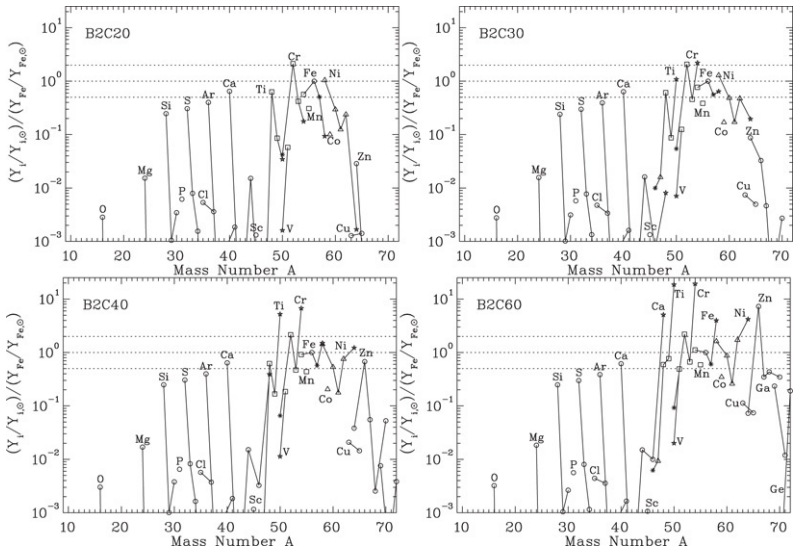

Fig. 5. Abundance ratios in comparison to solar values for a series of central ignition densities of 2–6 $\times$ 10^9 g cm^{-3} (the models B2C20-60). While ignition densities in the range (2–3)$\times 10^9$ g cm^{-3} lead to relative solar abundance ratios in the Fe-group, higher ignition densities can explain overabundances of ^{48}Ca, ^{50}Ti, ^{54}Cr, ^{58}Fe, ^{64}Ni, and ^{66}Zn. They should happen occasionally to account for these isotopes [90].

the accretion history within the progenitor binary system, and (c) the central ignition density (determined by the binary accretion history) can implicitly be affected by the metallicity [39].

5. Core collapse supernovae

5.1. Intermediate-mass elements and the Fe-group

Observations show typical kinetic energies of 10^{51} erg in supernova remnants. This permits one to perform light curve as well as explosive nucleosynthesis calculations by introducing a shock of appropriate energy in the pre-collapse stellar model [107,89,68,35,65,82,70]. Such induced calculations lack self-consistency and cannot predict the ejected ^{56}Ni-masses from the innermost explosive Si burning layers (powering the supernova light curves by the decay chain ^{56}Ni–^{56}Co–^{56}Fe) due to missing knowledge about the detailed explosion mechanism, and therefore the mass cut between the neutron star and supernova ejecta. However, the intermediate mass elements Si–Ca are only dependent on the explosion energy and the stellar structure of the progenitor star, while abundances for elements like O and Mg are essentially determined by the stellar progenitor's evolution. Thus, when moving in from the outermost to the innermost ejecta of an SN II explosion, we see an increase in the complexity of our understanding, depending (a) only on stellar evolution, (b) on the stellar evolution and the explosion energy, and (c) on stellar evolution and the complete explosion mechanism.

The correct prediction of the amount of Fe-group nuclei ejected (which includes also one of the so-called alpha-elements, i.e. Ti) and their relative composition depends directly on the explosion mechanism and the size of the Fe-core. Three types of uncertainties are inherent in the Fe-group ejecta, related to (i) the total amount of Fe(group) nuclei and the mass cut between neutron star and ejecta, mostly measured by ^{56}Ni decaying to ^{56}Fe, (ii) the total explosion energy

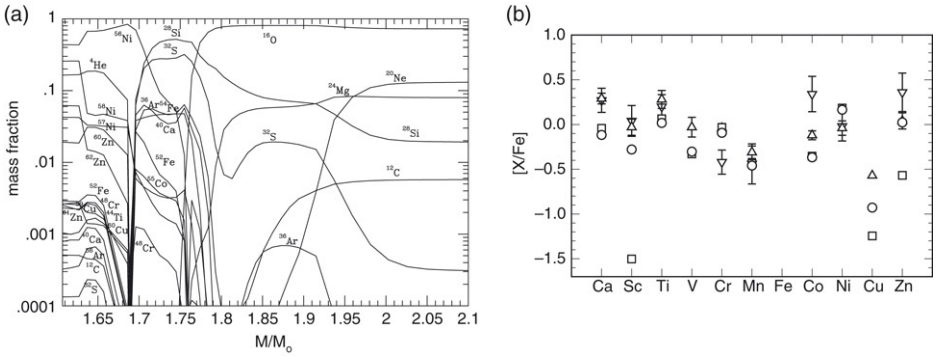

Fig. 6. *Left panel:* Results for the composition of supernova ejecta from an induced explosion calculation of a 20 $M_\odot$ star [89]. The change of the Fe-group composition in the innermost ejecta is due to the change in the Y_e of the precollapse stellar model. *Right panel:* Comparson of these abundances (open squares) with abundance observations of low metallicity stars (triangles [28,13]), which reflect average type II supernova ejecta. Calculations which include also neutrino interactions during the explosion (open circles) [26], lead to proton-rich conditions in the innermost zones and an improved description of the iron group abundances (see Sc and Zn). Cu is an s-process element and originates from other sources.

which influences the entropy of the ejecta and with it the amount of radioactive ^{44}Ti as well as ^{48}Cr (decaying to ^{48}Ti and being responsible for elemental Ti), and finally (iii) the neutron richness or $Y_e = \langle Z/A \rangle$ of the ejecta, dependent on stellar structure, electron captures, and neutrino interactions [26]. The electron fraction Y_e influences strongly the overall Ni/Fe ratio.

An example for the composition after explosive processing due to an (induced) shock wave is shown in Fig. 6(a), taken from [89]. The outer ejected layers ($M(r) > 2\ M_\odot$) are unprocessed by the explosion and contain results of prior H-, He-, C-, and Ne-burning during stellar evolution. The interior parts of SNe II contain products of explosive Si, O, and Ne burning. In the inner ejecta, which experience explosive Si-burning, Y_e changes from 0.4989 to 0.494. This Y_e originates from beta-decays and electron captures in the pre-explosive hydrostatic fuel of these layers. Consequently huge changes occur in the Fe-group composition for mass zones below $M(r) = 1.63\ M_\odot$. There, the abundances of ^{58}Ni and ^{56}Ni become comparable. All neutron-rich isotopes increase (^{57}Ni, ^{58}Ni, ^{59}Cu, ^{61}Zn, ^{62}Zn), the even-mass isotopes (^{58}Ni, ^{62}Zn) show the strongest effect. One can recognize the increase of ^{60}Zn, ^{52}Fe, ^{48}Ce, and ^{44}Ti for the inner high entropy zones, but also a reduction of the $N = Z$ nuclei in the more neutron-rich layers. More details can be found in extended discussions [89,65]. Neutrino reactions during the explosion were not yet included in these induced explosion calculations that utilized a thermal bomb prescription.

5.2. The νp-process

The influence of neutrino interactions on supernova nucleosynthesis has been emphasized for many years [18]. Recent core collapse supernova simulations with accurate neutrino transport [53,11,93] show the presence of proton-rich neutrino heated matter, both in the inner ejecta [53,11] and the early neutrino wind from the proto-neutron star [11]. This matter, part of the initially shock-heated material located between the surface of the proto-neutron star and the shock front expanding through the outer layers, is subject to a large neutrino energy deposition, heating the matter. This and the expansion, lifting the electron degeneracy, make it possible for the reactions $\nu_e + n \leftrightarrow p + e^-$ and $p + \overline{\nu}_e \leftrightarrow n + e^+$ (i.e. neutrino and antineutrino captures on free nucleons and their inverse reactions, electron and positron capture) to engender the composition

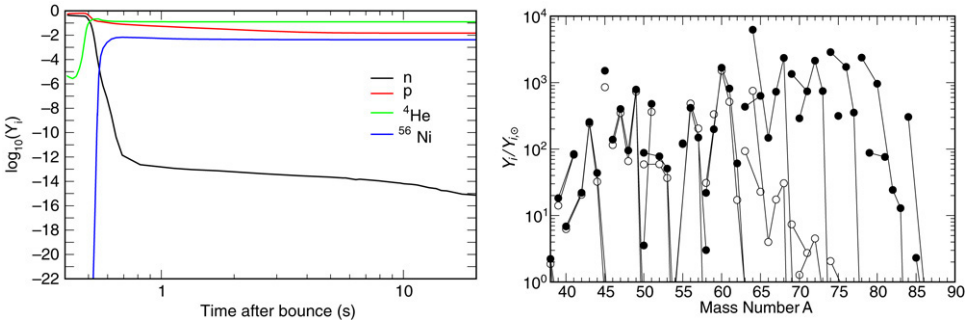

Fig. 7. *Left panel:* Evolution of the abundance of neutrons, protons, alpha-particles, and ^{56}Ni in a nucleosynthesis trajectory resulting from model B07 of Ref. [26]. *Right panel:* Isotopic abundances for model B07 of Ref. [26] relative to solar abundances [56] (filled circles), compared with earlier predictions [89] (open circles). The filled circles represent calculations where (anti)neutrino absorption reactions are included in the nucleosynthesis, while for the open circles neutrino interactions are neglected. The effect of neutrino interactions is clearly seen for nuclei above $A > 64$, where enhanced abundances are obtained.

proton-rich [25,77,26], with an electron fraction $Y_e > 0.5$. This effect will always be present in successful explosions with ejected matter irradiated by a strong neutrino flux, independent of the details of the explosion. While this matter expands and cools, nuclei can form resulting in a composition dominated by $N = Z$ nuclei, mainly ^{56}Ni and ^{4}He, and protons. Without the further inclusion of neutrino and antineutrino reactions, the composition of this matter will finally consist of protons, alpha-particles, and heavy (Fe-group) nuclei, i.e. a proton- and alpha-rich freeze-out that results in enhanced abundances of ^{45}Sc, ^{49}Ti, and ^{64}Zn [25,77,26].

Traditional explosive (supernova) nucleosynthesis calculations did not include interactions with neutrinos and antineutrinos. The heaviest nuclei synthesized in these calculations have a mass number $A = 64$. The matter flow stops at the nucleus ^{64}Ge, which has a small proton capture probability and a beta-decay half-life (64 s) that is much longer than the expansion time scale (10 s) [77]. When reactions with neutrinos and antineutrinos are considered for both free and bound nucleons, the situation becomes dramatically different [27,76,102]. $N \sim Z$ nuclei are practically inert to neutrino capture (converting a neutron into a proton), because such reactions are endoergic for neutron-deficient nuclei located away from the valley of stability. The situation is different for antineutrinos that are captured in a typical time of a few seconds, both on protons and on nuclei, at the distances at which nuclei form (∼1000 km). As protons are more abundant than heavy nuclei, antineutrino capture occurs predominantly on protons, causing a residual density of free neutrons of 10^{14}–10^{15} cm^{-3} for several seconds when the temperatures are in the range 1–3 $\times$ 10^9 K. This effect is clearly seen in Fig. 7 (left panel), where the time evolution of the abundances of protons, neutrons, alpha-particles and ^{56}Ni are shown for a trajectory of model B07 of [26]. The solid (dashed) lines display the nucleosynthesis results, which include (omit) neutrino and antineutrino absorption interactions after nuclei are formed. ^{56}Ni serves to illustrate when nuclei are formed. The difference in proton abundances between both calculations is due to antineutrino captures on protons, producing neutrons which drive the νp-process. Without the inclusion of antineutrino captures, the neutron abundance soon becomes too small to allow for any capture on heavy nuclei.

The neutrons produced via antineutrino absorption on protons can easily be captured by neutron-deficient $N \sim Z$ nuclei (for example ^{64}Ge), which have large neutron capture cross sections. While proton capture, (p, γ), on ^{64}Ge takes too long or is impossible, the (n, p) reaction

dominates, permitting the matter flow to continue to nuclei heavier than ^{64}Ge via subsequent proton captures with a freeze-out close to 10^9 K. Fig. 7 (right panel) shows the results for the composition of supernova ejecta from one hydrodynamical model described in [26], which includes neutrino absorption reactions in the nucleosynthesis calculations (filled circles) that lead initially to proton-rich conditions in the innermost zones, experiencing afterwards the νp-process. These abundances are compared to our earlier nucleosynthesis calculations [89] (open circles) that did not include neutrino interactions, and therefore did not produce the proton-rich matter resulting from models with accurate neutrino transport [53,11,93].

5.3. Hypernovae

High mass stars (as discussed in Section 3) will lead to direct black hole formation or black hole formation via fallback onto the initially formed neutron star. Accretion phenomena onto stellar mass black holes (if the surroundings are of sufficiently low density) can cause a fireball behavior and be related to gamma-ray bursts or the collapsar/hypernova phenomenon [104,72,70,7]. They indicate higher explosion energies beyond 10^{52} erg, large ejected ^{56}Ni masses, and have been investigated extensively by [64,97]. While the general explosive nucleosynthesis behavior is similar to supernovae (see Fig. 6), the higher explosion energy of hypernovae shifts both the complete Si-burning region ($T_{\rm peak} > 5 \times 10^9$ K with Co, Zn, V, and some Cr as products) and the incomplete Si-burning region ($4 \times 10^9 < T_{\rm peak} < 5 \times 10^9$ K with Cr and Mn as products after decay) outwards in mass. With this outwards shift of the boundary, the ratio of complete to incomplete Si-burning products becomes larger, and therefore higher ratios of [(Zn, Co, V)/Fe] and lower ratios of [(Mn, Cr)/Fe] are obtained [70]. Which fraction of high mass stars lead to such events is still uncertain, and depends on rotation and magnetic field effects.

5.4. The r-process in supernovae

High neutron densities and high temperatures (providing high energy photons) will lead to rapid neutron captures, and simultaneously, a large rate of photodisintegrations. In such environments, both reaction time scales ($\tau_{n,\gamma}, \tau_{\gamma,n}$) are much shorter than those for beta-decays (τ_β), and a balance or chemical equilibrium can be achieved between these processes ($n+(Z, A) \leftrightarrow (Z, A+1)+\gamma$), creating a distribution of isotopic abundances for a given Z. With a given neutron density n_n and temperature T, a maximum occurs at the same neutron separation energy S_n in each isotopic chain. The r-process "path" is then defined as connecting the isotopes with the maximum abundance in all isotopic chains by β-decays, transferring nuclei from one isotopic chain to the next and determining the speed with which heavy nuclei are formed. The location of the r-process path underscores why information on the properties of nuclei far from stability is so critical to understanding the r-process. To first order, the knowledge of S_n (or equivalently nuclear masses) determines the r-process path, while the knowledge of beta-decay half-lives determines the shape of the abundance curve [15,74,57,63]. In reality, individual neutron-capture cross-sections enter as well—especially during the freeze-out (disappearance) of neutrons when the temperatures drop (during expansion and cooling of supernova matter) and equilibrium conditions no longer prevail. Nuclei in the r-process path with the longest half-lives, of the order 0.2–0.3 s, are related to the abundance peaks—typical half-lives encountered between peaks are smaller by a factor of 10 to 100.

Given the fact that high neutron densities, as required for an r-process to occur, are hard to obtain suddenly in hydrostatic astrophysical settings, the logical conclusion is that realistic

astrophysical sites are related to explosive environments. In such a case, neutron number densities and temperatures (and thus also the $S_n(Z)$ of the r-process path) are not constant as a function of time, and the abundance curve observed relates only to the r-process path at the moment of neutron freeze-out. The next question is that of which type of explosive burning leads to initially high temperatures, producing Fe-group or heavier nuclei, with a leftover of neutrons per (heavy target) seed nucleus in order to synthesize nuclei with $A > 200$. This requires an about 150 neutrons per r-process seed, starting from Fe-nuclei or somewhat beyond. There have been a number of investigations, testing which conditions for a heated blob of material in astrophysical events with entropy S, initial neutron/proton or more generally proton/nucleon ratio Y_e, combined with a timescale of a (close to) adiabatic expansion, can fulfill this requirement [22]. The results are connected to the behavior of explosive Si-burning and the so-called freeze-out of charged particle reactions at a temperature of the order 2–3 $\times$ 10^9 K, before an r-process sets in with capture of the remaining neutrons.

At low entropies (with a normal freeze-out of remaining Fe-group nuclei and nucleons), the required neutron/seed ratio is almost entropy-independent and requires a proton/nucleon ratio of $Y_e = \langle Z/A \rangle = 0.12$–$0.3$. Such a high neutron excess is only possible for high densities in neutron stars under beta-equilibrium ($e^- + p \leftrightarrow n + \nu$, $\mu_e + \mu_p = \mu_n$), based on the high electron Fermi energies which are comparable to the neutron–proton mass difference [60,23]. Deviations from this straightforward balance in the neutron/proton ratio are only possible if one stores large amounts of mass in $N = Z$ nuclei with small neutron capture cross sections (e.g. ^{4}He), leaving then all remaining neutrons for a few heavy seed nuclei. This phenomenon is known as an extremely α-rich freeze-out in complete Si-burning, and corresponds to a weak link of reactions between the light nuclei (n, p, α) and heavier nuclei at low densities. The entropy ($\propto T^3/\rho$ in radiation dominated matter) can be used as a measure of the ratio between the remaining He mass fraction and heavy nuclei. A well known case is the big bang, where under extreme entropies, essentially only ^{4}He is left as the heaviest nucleus available. Somewhat lower entropies permit the production of (still small) amounts of heavy seed nuclei. Then, even moderate values of $Y_e = 0.4$–0.5 can lead to high ratios of neutrons to heavy nuclei for entropies in excess of 200 k_B per baryon, and neutron captures can proceed to form the heaviest r-process nuclei [87,105,41,61,22]. This is thought to be related to the latest/innermost ejecta of type II supernovae in form of the so-called neutrino wind from the surface of the just formed proto-neutron star [78,91,88,92,108]. Conditions with an entropy of 190 k_B per baryon, a Y_e of 0.45 and an expansion timescale related to a mass zone residing at initially a radius of 130 km and expanding with a typical velocity of 7500 km/s, are perfect for reproducing the $A = 130$ r-process peak [19]. Due to the time-dependence of the initially very neutron-rich r-process path, the timescale for producing the $A = 130$ peak is only 0.15 s, in comparison to 1.7 s in calculations with a static r-process path.

It is not possible to obtain an overall global fit for one set of conditions. One rather needs a superposition of conditions to obtain a global fit to r-process abundances as found in the solar system. This can, in principle, be due to different zones in one astrophysical event, but might also be related to the combination of different events. While it was possible to find such a global superposition in static calculations [22,74], global superpositions of entropies face difficulties in reproducing the mass region 80–110 adequately [22,101], reflecting abundances determined by alpha separation energies after an alpha-rich freeze-out rather than neutron separation energies. Therefore, Fig. 8 shows only a superposition of high entropies (150, 190, 230, 250 and 274 k_B per nucleon) which reproduce the heavy r-process elements quite well, opposite to environments which can produce heavy nuclei, but with r-process paths too close to stability [24]. It is found that entropies beyond 270 lead to fission cycling, similar to conditions

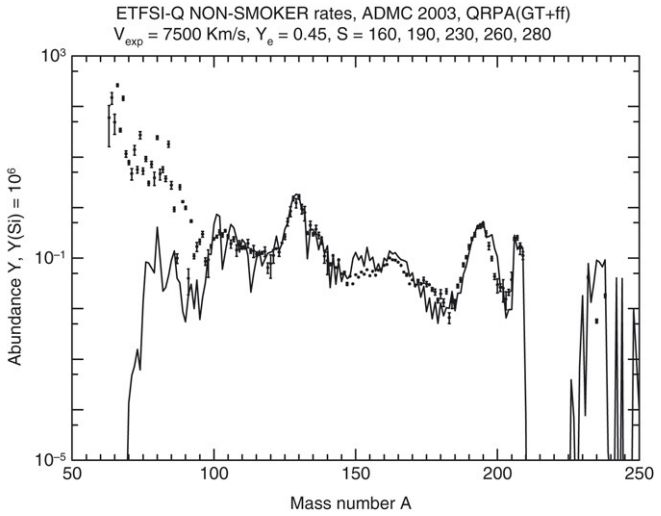

Fig. 8. Entropy superposition from 150 to 274 k_B per nucleon, which reproduces the heavy r-process abundances well ($A > 100$), including the pigmy peak in the rare earth region. The latter is well reproduced when neutron captures are followed fully [79], and also after the freeze-out from chemical equilibrium between neutron captures and photodisintegrations [19].

obtained in neutron star mergers [23], and neutron-induced as well as beta-delayed fission rates are required [73]. It remains to be seen which site is responsible the weak r-process component discussed above [103], and whether supernovae can account for the entropies required to reproduce the main component [91,92].

6. Evolution of galactic abundances

6.1. Galactic evolution

The first stars start with abundances from Big Bang Nucleosynthesis, being the relics of a hot and dense state of the early universe which underwent adiabatic expansion. The big bang contributed the light nuclides ^{1}H, ^{2}H, ^{3}He, ^{4}He, and ^{7}Li, whose abundances are determined by only one parameter, the entropy, expressible in terms of the baryon to photon ratio $\eta = n_B/n_\gamma$, because this initial state possesses also a weak interaction equilibrium, determining Y_e. The status of the relevant thermonuclear reactions has been discussed recently [58]. Major uncertainties are related to the determination of the primordial abundance of ^{2}H, ^{3,4}He and ^{7}Li with astronomical means, and their consistency with the constraint on η from WMAP microwave background observations [20,14].

The further abundance evolution is related to the input of stellar events. Explosive nucleosynthesis yields leave fingerprints in spectra, light curves, X-rays and radioactivities/decay gamma-rays of individual events for the explosive outbursts as well as their remnants. Galactic chemical evolution is thus a global test for all contributing stellar yields, especially ejecta of SNe II and SNe Ia, if we are mainly concerned with intermediate-mass and heavy elements [3, 21,4]. In the following, want to confront the expectations resulting from the yield predictions presented in Sections 4 and 5 with observational data (see Fig. 9). Before doing so, we give short discussions of the expected rates of these events and the possible direct/indirect metallicity dependence of the events and their yields.

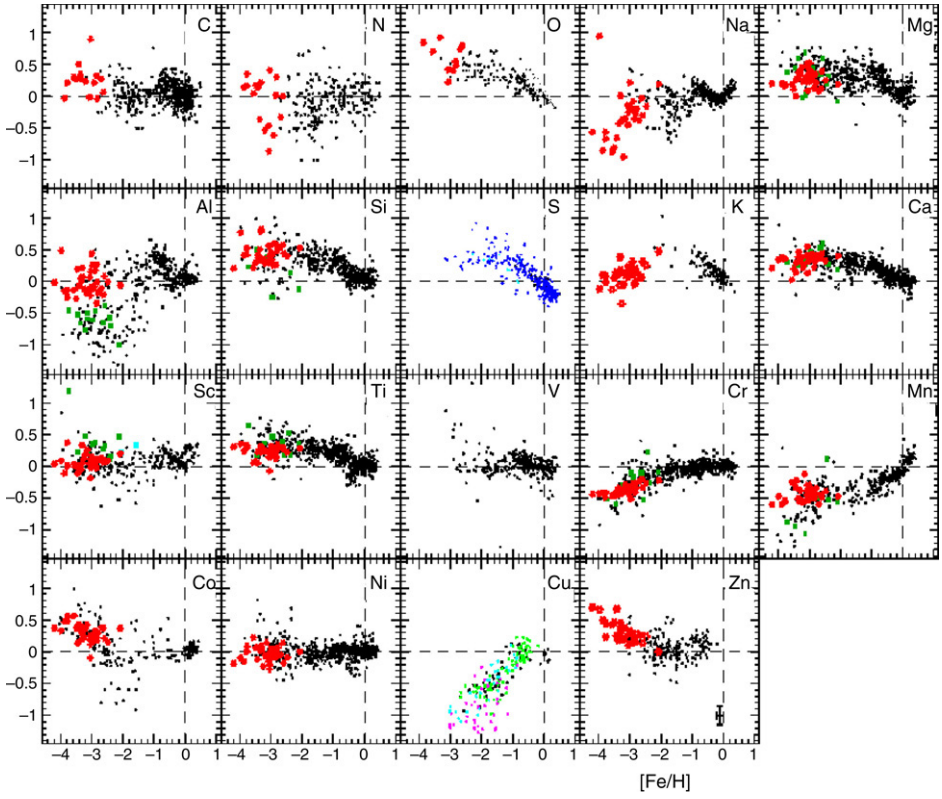

Fig. 9. Abundance ratios $[X/Fe] = \log_{10}[(X/Fe)/(X/Fe)_{\odot}]$ for various elements from C to Zn as a function of metallicity [Fe/H] in stars of the Milky Way. Small data points represent various observational sources collected by Prantzos (2005, private communication); large data points at low metallicitiy are from a recent VLT survey [13]. A typical uncertainty is indicated by the error bar in the last frame.

Supernova rates: The chemical evolution of galaxies is dominated by contributions from SNe II and SNe Ia. Early in galactic evolution, massive stars will dominate due to their short evolution timescales. The death of these massive stars results correspondingly in a large type II+type Ib/c supernova rate. The longer lifetime of intermediate mass stars (leading to white dwarfs), and the required mass transfer in binary systems, delays the onset of type Ia supernovae. For further details see Figure 39 in [94]. Such chemical evolution calculations indicate the strong influence of SNe Ia starting at metallicities of about $[Fe/H] = -1$. The present type II+type Ib/c supernova rate is estimated to be 2.4–2.7 per century, while the type Ia rate is 0.3–0.6 per century [100]. Thus, the total rate amounts to about 3 per century, while the ratio of core collapse (type II+type Ib) to thermonuclear (type Ia) is about 6, or inversely Ia/(II+Ib) = 0.167. This will play a role for the relative Fe-group contribution from both supernova types.

6.2. Supernova contributions

General Fe-group contribution: For a slightly low SN Ia frequency of type Ia/(II+Ib) = 0.15 and typical W7 type abundances for SNe Ia [69,44,9], ^{56}Fe from SNe Ia amounts to about 55% of the total ^{56}Fe. Larger Ia/(Ib+Ic) ratios would increase this contribution, leading to estimates

for the contributions to Fe and Fe-group elements from SNe II and SNe Ia to be $\sim 1/3$ and $\sim 2/3$, respectively [75]. Other Fe-group elements are co-produced with Fe. Their ratio could be different in SNe Ia and SNe II, and could be dependent on metallicities as well. This would reflect the evolution of [X/Fe]. The fact that [Sc, V, Cr, Co, Ni, Zn/Fe] remains constant, and equal to its solar value for metalicities down to about -2, indicates that both SNe Ia and II/Ibc reproduce these elements on average in solar proportions, as discussed in Sections 4 and 5. Especially the abundances of Sc and Zn can now be explained by the effect of neutrinos in the innermost ejected zones of SNe II. Lower metallicity effects remain to be discussed.

Alpha elements: Alpha elements (O, Ne, Mg, Si, S, Ar, Ca) are enhanced in comparison to Fe in SNe II (as seen in low metallicity stars and expected from Section 5). To obtain solar abundance ratios for combined nucleosynthesis products near solar metallicity, this overabundance of alpha elements in SNe II has to be compensated for by a higher Fe to alpha element ratios in SNe Ia (as seen in Section 4). The ratio of alpha elements to Fe, $[\alpha/\mathrm{Fe}]$, is found to be constant above its solar value at low metallicities, and to slowly decline to the solar value at about $[\mathrm{Fe/H}] = -1$.

Indirect metallicity effects: The evolution of a single massive star, i.e. its explosion mechanism and therefore its nucleosynthesis, is determined by the core size, which in turn depends on its initial mass, rotation, and metallicity. For a given initial mass, the mass of the C/O-core decreases with increasing metallicity due to stronger mass loss [32] (see Fig. 3(a)). This has the effect that with decreasing metallicity in galactic evolution, the explosive nucleosynthesis results are shifted towards those of larger C–O-cores (or if we speak in simple terms the explosive Nucleosynthesis, products of more massive supernovae start to dominate).

While the typical explosion energy of core collapse supernovae is of the order of 10^{51} erg, very probably individual events will show variations. Studies of explosions due to neutrino absorption exhibit a twofold behavior (see Fig. 3(b)): the explosion energy increases steadily with progenitor mass, peaking around a progenitor masses of $\sim 25\ \mathrm{M}_\odot$, with a fast decline thereafter. For progenitors beyond $\sim 40\ \mathrm{M}_\odot$ no explosions are observed, corresponding to a direct black hole formation. If one combines this apparent increase of explosion energy with progenitor mass with the metallicity effect discussed above, one expects on average an increase in explosion energy for the core collapse supernovae contributing to a very low metallicity galactic evolution. This would alter nucleosynthesis products on average, similar to the discussion of hypernovae in Section 5, i.e. higher ratios of [(Zn, Co, V)/Fe] and lower ratios of [(Mn, Cr)/Fe] are obtained.

V, Cr, Mn, Co, and Zn: Mn seems on average to be somewhat underproduced below $[\mathrm{Fe/H}] = -1$, i.e. by SNe II and overproduced by SNe Ia, in order to attain solar values at $[\mathrm{Fe/H}] = 0$. All the other elements show typically a solar behavior down to $[\mathrm{Fe/H}] = -3$. At very low metallicities, exactly those deviations occur, which are discussed in the previous paragraph. That is, we seem to see explosive nucleosynthesis results of explosions with increasing energy. There are three explanations, which might act in combination: (a) the implicit metallicity effect discussed above, (b) hypernova nucleosynthesis as first explosive nucleosynthesis events, and (c) correlated inhomogeneities. Metallicities of $[\mathrm{Fe/H}] = -3$ can be attained if a single supernova pollutes pristine material of the order of $10^4\ \mathrm{M}_\odot$. At such early times, the interstellar medium is not well mixed. We could just see the effects of single supernovae/hypernovae for $[\mathrm{Fe/H}] < -3$. As with inceasing explosion energy, the amount of interstellar medium (mostly H) with which the ejecta are mixed, increases, increasing explosion energies cause smaller [Fe/H]. Thus, one would also expect increasing deviations of V, Cr, Mn, Co, and Zn, just as observed.

Sr, Y, Zr: The production of elements beyond iron is traditionally attributed to two neutron capture processes: the s-process (slow process) and the r-process (rapid process). The s-process moves

along the valley of stability of β-stability and requires low neutron densities ($n_n < 10^8$ cm^{-3}). This process builds about half the nuclides from Fe to Bi, in particular the elements Sr, Y, Zr, Ba to Nd, and Pb (corresponding to the three main s-process peaks). Asymptotic giant branch (ABG) star nucleosynthesis for a variety of metallicities and ^{13}C pocket efficiencies show a strong decrease in the production efficiency with decreasing metallicity [95]. Summing all the contributions to the elements Sr, Y, and Zr, there are major fractions of the solar Sr, Y, and Zr missing at low metallicities. These missing fractions are expected not to be of s-process but rather of primary origin, resulting from all massive stars. Recent galactic chemical evolution studies [95] suggest the existence of a *lighter element primary process*, operating very early in the galaxy and being independent of the r-process, to explain the observed trends and scatter of Sr, Y, and Zr at very low metalicities. The *νp*-process, discussed in Section 5, could solve this puzzle [27,76], and is also expected to explain the light p-elements deficiencies found in p-process calculations [99].

r-process elements: There are detailed observations of the r-process element Eu which show a very large star-to-star scatter in the Eu/Fe abundances—a factor of about 200 at low metallicities [85]. This scatter diminishes dramatically at higher metallicites. A likely explanation for these trends is that at early times (and low metallicities) the galaxy was chemically inhomogeneous, with some regions containing larger amounts of r-process ejecta (in comparison to Fe) than others. At later times, these differences in the total abundance seem to vanish, but rather late in galactic evolution. As r-process elements are seen already at very low metallicities of about [Fe/H] $= -3$, high mass stars turning into core collapse supernovae are identified as an r-process site. But this seems inconsistent with all supernovae being involved, and probably a very restricted mass range or other selection effects like rotation and/or magnetic fields make the main r-process a rare event [92].

References

[1] C. Angulo, et al., Nuclear Phys. A 656 (1999) 3.
[2] M. Arnould, S. Goriely, Nuclear Phys. A 777 (2006) 157.
[3] D. Argast, M. Samland, F.-K. Thielemann, O.E. Gerhard, Astronom. Astrophys. 388 (2002) 842.
[4] D. Argast, M. Samland, F.-K. Thielemann, Y.-Z. Qian, Astronom. Astrophys. 416 (2004) 997.
[5] M. Asplund, N. Grevesse, J. Sauval, Nuclear Phys. A 777 (2006) 1.
[6] Z.Y. Bao, H. Beer, F. Kappeler, et al., At. Data Nucl. Data Tables 76 (2000) 70.
[7] S. Blinnikov, Surv. High Energy Phys. 20 (2006) 89.
[8] I.N. Borzov, Nuclear Phys. A 777 (2006) 645.
[9] F. Brachwitz, D.J. Dean, W.R. Hix, K. Iwamoto, K. Langanke, G. Martínez-Pinedo, K. Nomoto, M.R. Strayer, F.-K. Thielemann, H. Umeda, Astrophys. J. 536 (2000) 934.
[10] L.R. Buchmann, C.A. Barnes, Nuclear Phys. A 777 (2006) 254.
[11] R. Buras, M. Rampp, H.-T. Janka, K. Kifonidis, Phys. Rev. Lett. 90 (2003) 241101.
[12] A. Burrows, S. Reddy, T.A. Thompson, Nuclear Phys. A 777 (2006) 356.
[13] R. Cayrel, E. Depagne, M. Spite, V. Hill, F. Spite, P. François, B. Plez, T. Beers, F. Primas, J. Andersen, B. Barbuy, P. Bonifacio, P. Molaro, B. Nordström, Astronom. Astrophys. 416 (2004) 1117.
[14] A. Coc, E. Vangioni-Flam, P. Descouvemont, A. Adahchour, C. Angulo, Astrophys. J. 600 (2004) 544.
[15] J.J. Cowan, F.-K. Thielemann, J.W. Truran, Phys. Rep. 208 (1991) 267.
[16] P. Descouvemont, T. Rauscher, Nuclear Phys. A 777 (2006) 137.
[17] I. Domínguez, P. Höflich, O. Straniero, Astrophys. J. 557 (2001) 279.
[18] G.V. Domogatsky, D.K. Nadyozhin, Sov. Astron. 22 (1978) 297.
[19] K. Farouqi, Ph.D. Thesis, University of Mainz, 2005, unpublished.
[20] B.D. Fields, K.A. Olive, Nuclear Phys. A 777 (2006) 208.
[21] P. François, F. Matteucci, R. Cayrel, M. Spite, F. Spite, C. Chiappini, Astronom. Astrophys. 421 (2004) 613.
[22] C. Freiburghaus, et al., Astrophys. J. 516 (1999) 381.

[23] C. Freiburghaus, S. Rosswog, F.-K. Thielemann, Astrophys. J. 525 (1999) L121.
[24] C.L. Fryer, F. Herwig, A. Hungerford, F.X. Timmes, Astrophys. J. 646 (2006) L131.
[25] C. Fröhlich, P. Hauser, M. Liebendörfer, et al., Nuclear Phys. A 758 (2005) 27.
[26] C. Fröhlich, P. Hauser, M. Liebendörfer, G. Martínez-Pinedo, F.-K. Thielemann, E. Bravo, N.T. Zinner, W.R. Hix, K. Langanke, A. Mezzacappa, K. Nomoto, Astrophys. J. 637 (2006) 415.
[27] C. Fröhlich, G. Martínez-Pinedo, M. Liebendörfer, F.-K. Thielemann, E. Bravo, W.R. Hix, K. Langanke, N.T. Zinner, Phys. Rev. Lett. 96 (2006) 142502.
[28] R.G. Gratton, C. Sneden, Astronom. Astrophys. 241 (1991) 501.
[29] W.C. Haxton, P.D. Parker, C.E. Rolfs, Nuclear Phys. A 777 (2006) 226.
[30] A. Heger, C.L. Fryer, S.E. Woosley, N. Langer, D.H. Hartmann, Astrophys. J. 591 (2003) 288.
[31] W. Hillebrandt, J.C. Niemeyer, Ann. Rev. of Astron. & Astrophys. 38 (2000) 191.
[32] R. Hirschi, G. Meynet, A. Maeder, Astronom. Astrophys. 443 (2005) 581.
[33] W.R. Hix, B.S. Meyer, Nuclear Phys. A 777 (2006) 188.
[34] W.R. Hix, F.-K. Thielemann, Astrophys. J. 511 (1999) 862.
[35] R.D. Hoffman, S.E. Woosley, T.A. Weaver, T. Rauscher, F.-K. Thielemann, Astrophys. J. 521 (1999) 735.
[36] P. Hoeflich, A. Khokhlov, Astrophys. J. 457 (1996) 500.
[37] P. Höflich, C. Gerardy, E. Linder, et al., Lecture Notes in Phys. 635 (2003) 203.
[38] P. Höflich, K. Nomoto, H. Umeda, J.C. Wheeler, Astrophys. J. 528 (2000) 590.
[39] P. Höflich, Nuclear Phys. A 777 (2006) 579.
[40] P. Höflich, J.C. Wheeler, F.-K. Thielemann, Astrophys. J. 495 (1998) 617.
[41] R.D. Hoffman, et al., Astrophys. J. 482 (1997) 951.
[42] I.J. Iben, Astrophys. J. Suppl. 76 (1991) 55.
[43] C. Iliadis, et al., Astrophys. J. Suppl. 134 (2001) 151.
[44] K. Iwamoto, F. Brachwitz, K. Nomoto, N. Kishimoto, H. Umeda, W.R. Hix, F.-K. Thielemann, Astrophys. J. Suppl. 125 (1999) 439.
[45] F. Käppeler, F.-K. Thielemann, M. Wiescher, Ann. Rev. Nucl. Part. Sci. 48 (1998) 175.
[46] F. Käppeler, A. Mengoni, Nuclear Phys. A 777 (2006) 291.
[47] A.M. Khokhlov, P.A. Höflich, E.S. Oran, J.C. Wheeler, L. Wang, A.Y. Chtchelkanova, Astrophys. J. Lett. 524 (1999) L107.
[48] E. Kolbe, K. Langanke, G. Martinez-Pinedo, P. Vogel, J. Phys. G 29 (2003) 2569.
[49] K. Langanke, G. Martínez-Pinedo, Nuclear Phys. A 673 (2000) 481.
[50] K. Langanke, G. Martinez-Pinedo, Rev. Modern Phys. 75 (2003) 819.
[51] K. Langanke, F.-K. Thielemann, M. Wiescher, Lecture Notes in Phys. 651 (2004) 383.
[52] J.M. Lattimer, M. Prakash, Nuclear Phys. A 777 (2006) 479.
[53] M. Liebendörfer, A. Mezzacappa, F.-K. Thielemann, O.E. Messer, W.R. Hix, S.W. Bruenn, Phys. Rev. D 63 (2001) 103004.
[54] M. Liebendörfer, A. Mezzacappa, O.E.B. Messer, G. Martinez-Pinedo, W.R. Hix, F.-K. Thielemann, Nuclear Phys. A 719 (2003) 144.
[55] M. Liebendörfer, O.E.B. Messer, A. Mezzacappa, S.W. Bruenn, C.Y. Cardall, F.-K. Thielemann, Astrophys. J. Suppl. 150 (2004) 263.
[56] K. Lodders, Astrophys. J. 591 (2003) 1220.
[57] D. Lunney, J.M. Pearson, C. Thibault, Rev. Modern Phys. 75 (2003) 1021.
[58] L.E. Marcucci, K.M. Nollet, R. Schiavilla, R.B. Wiringa, Nuclear Phys. A 777 (2006) 111.
[59] G. Martinez-Pinedo, M. Liebendörfer, D. Frekers, Nuclear Phys. A 777 (2006) 395.
[60] B.S. Meyer, Astrophys. J. 343 (1989) 254.
[61] B.S. Meyer, et al., Phys. Rev. C 58 (1998) 3696.
[62] G. Meynet, A. Maeder, Astronom. Astrophys. 429 (2005) 581.
[63] P. Möller, B. Pfeiffer, K.-L. Kratz, Phys. Rev. C 67 (2003) 055802.
[64] T. Nakamura, H. Umeda, K. Iwamoto, K. Nomoto, M. Hashimoto, W.R. Hix, F.-K. Thielemann, Astrophys. J. 555 (2001) 880.
[65] T. Nakamura, H. Umeda, K. Nomoto, F.-K. Thielemann, A. Burrows, Astrophys. J. 517 (1999) 193.
[66] J.C. Niemeyer, Astrophys. J. 523 (1999) L57.
[67] K. Nomoto, et al., in: J.C. Niemeyer, J.W. Truran (Eds.), Type Ia Supernovae, Theory and Cosmology, Cambridge University Press, 2000, p. 63.
[68] K. Nomoto, M. Hashimoto, T. Tsujimoto, F.-K. Thielemann, N. Kishimoto, Y. Kubo, N. Nakasato, Nuclear Phys. A 616 (1997) 79.

[69] K. Nomoto, F.-K. Thielemann, K. Yokoi, Astrophys. J. 286 (1984) 644.
[70] K. Nomoto, N. Tominaga, H. Umeda, C. Kobayashi, K. Maeda, Nuclear Phys. A 777 (2006) 424.
[71] P. Nugent, E. Baron, D. Branch, A. Fisher, P.H. Hauschildt, Astrophys. J. 485 (1997) 812.
[72] B. Paczynski, Astrophys. J. 494 (1998) L45.
[73] I.V. Panov, E. Kolbe, B. Pfeiffer, T. Rauscher, K.-L. Kratz, F.-K. Thielemann, Nuclear Phys. A 747 (2005) 633.
[74] B. Pfeiffer, K.-L. Kratz, F.-K. Thielemann, W.B. Walters, Nuclear Phys. A 693 (2001) 282.
[75] N. Prantzos, Nuclear Phys. A 758 (2005) 249.
[76] J. Pruet, R.D. Hoffman, S.E. Woosley, H.-T. Janka, R. Buras, Astrophys. J. 644 (2006) 1028.
[77] J. Pruet, S.E. Woosley, R. Buras, H.-T. Janka, R.D. Hoffman, Astrophys. J. 623 (2005) 325.
[78] Y.-Z. Qian, S.E. Woosley, Astrophys. J. 471 (1996) 331.
[79] T. Rauscher, F.-K. Thielemann, At. Data Nucl. Data Tables 75 (2000) 1.
[80] T. Rauscher, et al., Nuclear Phys. A 675 (2000) 695.
[81] T. Rauscher, F.-K. Thielemann, At. Data Nucl. Data Tables 79 (2001) 47.
[82] T. Rauscher, A. Heger, R.D. Hoffman, S.E. Woosley, Astrophys. J. 576 (2002) 323.
[83] M. Reinecke, W. Hillebrandt, J.C. Niemeyer, Astronom. Astrophys. 391 (2002) 1167.
[84] F.K. Röpke, J.C. Niemeyer, W. Hillebrandt, Astrophys. J. 588 (2003) 952.
[85] C. Sneden, J.J. Cowan, Science 299 (2003) 70.
[86] O. Straniero, R. Gallino, S. Cristallo, Nuclear Phys. A 777 (2006) 311.
[87] K. Takahashi, J. Witti, H.-T. Janka, Astronom. Astrophys. 286 (1994) 857.
[88] M. Terasawa, et al., Astrophys. J. 578 (2002) L137.
[89] F.-K. Thielemann, K. Nomoto, M. Hashimoto, Astrophys. J. 460 (1996) 408.
[90] F.-K. Thielemann, F. Brachwitz, P. Höflich, G. Martinez-Pinedo, K. Nomoto, New Astronomy Rev. 48 (2004) 605.
[91] T.A. Thompson, A. Burrows, B.S. Meyer, Astrophys. J. 562 (2001) 887.
[92] T.A. Thompson, Astrophys. J. 585 (2006) L33.
[93] T.A. Thompson, E. Quataert, A. Burrows, Astrophys. J. 620 (2005) 861.
[94] F.X. Timmes, S.E. Woosley, T.A. Weaver, Astrophys. J. Suppl. 98 (1995) 617.
[95] C. Travaglio, R. Gallino, E. Arnone, J. Cowan, F. Jordan, C. Sneden, Astrophys. J. 601 (2004) 864.
[96] C. Travaglio, W. Hillebrandt, M. Reinecke, F.-K. Thielemann, Astronom. Astrophys. 425 (2004) 1029.
[97] H. Umeda, K. Nomoto, Astrophys. J. 619 (2005) 427.
[98] H. Umeda, K. Nomoto, H. Yamaoka, S. Wanajo, Astrophys. J. 513 (1999) 861.
[99] H. Utsonamiya, P. Mohr, A. Zilges, M. Rayet, Nuclear Phys. A 777 (2006) 459.
[100] S. van den Bergh, R.D. McClure, Astrophys. J. 425 (1994) 205.
[101] S. Wanajo, T. Kajino, G.J. Mathews, K. Otsuki, Astrophys. J. 554 (2001) 578.
[102] S. Wanajo, Astrophys. J. 647 (2006) 1323.
[103] G.J. Wasserburg, M. Busso, R. Gallino, K.M. Nollet, Nuclear Phys. A 777 (2006) 5.
[104] S.E. Woosley, Astrophys. J. 405 (1993) 273.
[105] S.E. Woosley, et al., Astrophys. J. 433 (1994) 229.
[106] S.E. Woosley, T.A. Weaver, in: S.A. Bludman, R. Mochkovitch, J. Zinn-Justin (Eds.), Supernovae, 1994, p. 63.
[107] S.E. Woosley, T.A. Weaver, Astrophys. J. Suppl. 101 (1995) 181.
[108] T. Yoshida, T. Terasawa, T. Kajino, K. Sumiyoshi, Astrophys. J. 600 (2004) 204.